Article

Cell Reports

Stress-Induced CDK5 Activation Disrupts Axonal Transport via Lis1/Ndel1/Dynein

Graphical Abstract

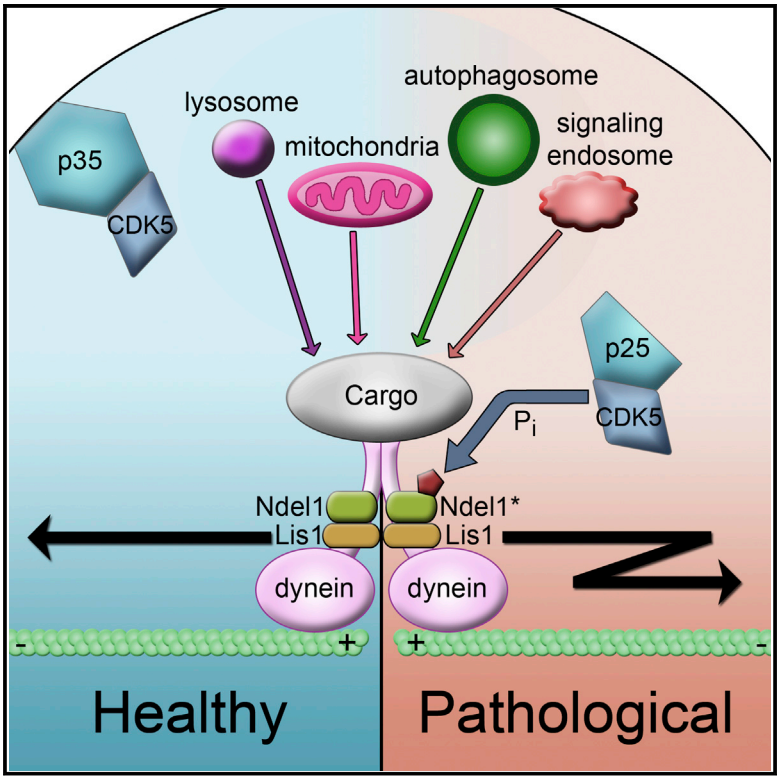

Authors

Eva Klinman, Erika L.F. Holzbaur

Correspondence

holzbaur@mail.med.upenn.edu

In Brief

Klinman and Holzbaur demonstrate that stress-induced activation of cyclin-dependent kinase 5 (CDK5) misregulates transport of a wide range of cargos via a Lis1/Ndel1-dependent mechanism, and they show that reduction of CDK5 activity in neurons from SOD1^{G93A} mice rescues the observed transport deficits.

Highlights

- Activated CDK5 disrupts transport of a range of cargos
- CDK5 acts through the Lis1/Ndel1 complex to regulate dynein
- Reduction of CDK5 activity in neurons from an ALS mouse model rescues transport

Klinman & Holzbaur, 2015, Cell Reports *12*, 462–473
July 21, 2015
http://dx.doi.org/10.1016/j.celrep.2015.06.032

CellPress

OPEN ACCESS
CellPress

Cell Reports
Article

Stress-Induced CDK5 Activation Disrupts Axonal Transport via Lis1/Ndel1/Dynein

Eva Klinman[1] and Erika L.F. Holzbaur[1,*]
[1]Neuroscience Graduate Group and Department of Physiology, Perelman School of Medicine, University of Pennsylvania, Philadelphia, PA 19104-6085, USA
*Correspondence: holzbaur@mail.med.upenn.edu
http://dx.doi.org/10.1016/j.celrep.2015.06.032

SUMMARY

Axonal transport is essential for neuronal function, and defects in transport are associated with multiple neurodegenerative diseases. Aberrant cyclin-dependent kinase 5 (CDK5) activity, driven by the stress-induced activator p25, also is observed in these diseases. Here we show that elevated CDK5 activity increases the frequency of nonprocessive events for a range of organelles, including lysosomes, autophagosomes, mitochondria, and signaling endosomes. Transport disruption induced by aberrant CDK5 activation depends on the Lis1/Ndel1 complex, which directly regulates dynein activity. CDK5 phosphorylation of Ndel1 favors a high affinity Lis1/Ndel/dynein complex that blocks the ATP-dependent release of dynein from microtubules, inhibiting processive motility of dynein-driven cargo. Similar transport defects observed in neurons from a mouse model of amyotrophic lateral sclerosis are rescued by CDK5 inhibition. Together, these studies identify CDK5 as a Lis1/Ndel1-dependent regulator of transport in stressed neurons, and suggest that dysregulated CDK5 activity contributes to the transport deficits observed during neurodegeneration.

INTRODUCTION

Axonal transport is essential to maintain neuronal viability, yet the molecular mechanisms that regulate transport are not yet understood. The coordinated activities of anterograde-directed kinesins and retrograde-directed dynein motors drive transport in neurons. Motor activity is regulated by multiple mechanisms, leading to efficient long-distance transport and the specific targeting of organelles to appropriate locations (Fu and Holzbaur, 2014; Hancock, 2014; Maday et al., 2014).

One kinase proposed to regulate axonal transport is cyclin-dependent kinase 5 (CDK5) (Goodwin et al., 2012; Ou et al., 2010; Pandey and Smith, 2011). While most cyclin-dependent kinases regulate the cell cycle (Dhariwala and Rajadhyaksha, 2008), CDK5 expression is limited to post-mitotic cells including neurons (Tsai et al., 1993). The primary activator of neuronal CDK5 is p35. The CDK5/p35 complex is both temporally and spatially regulated; the active complex remains bound to the plasma membrane and is inactivated within 20 min via CDK5-dependent phosphorylation of p35 (Figure 1A), which targets p35 for ubiquitination and proteosomal degradation (Dhavan and Tsai, 2001; Kusakawa et al., 2000; Patrick et al., 1998).

The CDK5/p35 complex plays an important role in neuronal development and migration, but its function in mature neurons is less well understood (Modi et al., 2012; Su and Tsai, 2011). Multiple studies have implicated CDK5 in the regulation of vesicle and organelle trafficking, with conflicting conclusions. In *C. elegans*, CDK5 regulates axodendritic sorting (Goodwin et al., 2012; Ou et al., 2010). In mice, CDK5 has been proposed to regulate the anterograde transport of organelles through a pathway involving glycogen synthase kinase 3 and kinesin (Morel et al., 2010; Morfini et al., 2004). Alternatively, CDK5 has been proposed to enhance the bidirectional transport of lysosomes via a mechanism involving nuclear distribution protein nudE-like 1 (Ndel1), Lis1, and dynein (Pandey and Smith, 2011). Ndel1 and Lis1 have been studied extensively in the context of lissencephaly; they form a complex that binds to and regulates cytoplasmic dynein (Huang et al., 2012; Wynshaw-Boris, 2007). Ndel1 is a known CDK5 phosphorylation target, suggesting a potential mechanism for the effects of CDK5 on dynein-mediated axonal transport.

Under conditions of cellular stress, including oxidative stress, ischemia, mitochondrial dysfunction, inflammation, or disease, CDK5 activity becomes misregulated. Calcium influx activates calpain, which cleaves p35 to a membrane-bound p10 subunit and a cytosolic p25 subunit (Figure 1A; Su and Tsai, 2011; Zhang et al., 2012). The p25 subunit retains the activation site for CDK5, but not the phosphorylation site necessary for ubiquitination and subsequent degradation. Thus, the p25/CDK5 complex displays sustained activation that is both temporally and spatially deregulated (Dhariwala and Rajadhyaksha, 2008).

The deregulation of CDK5 in stressed neurons suggests that aberrant CDK5 activity may contribute to neurodegeneration (Dhariwala and Rajadhyaksha, 2008). Both abnormal cellular localization and hyperactivation of CDK5 has been observed in neurons of patients with amyotrophic lateral sclerosis (ALS). This rise in CDK5 activity is accompanied by the accumulation of cargo in the cell body and proximal axon of both motor and sensory neurons in mouse models of ALS (Cozzolino et al., 2012; Shukla et al., 2012). Diverse cargo, including lysosomes, autophagosomes, mitochondria, and signaling molecules such

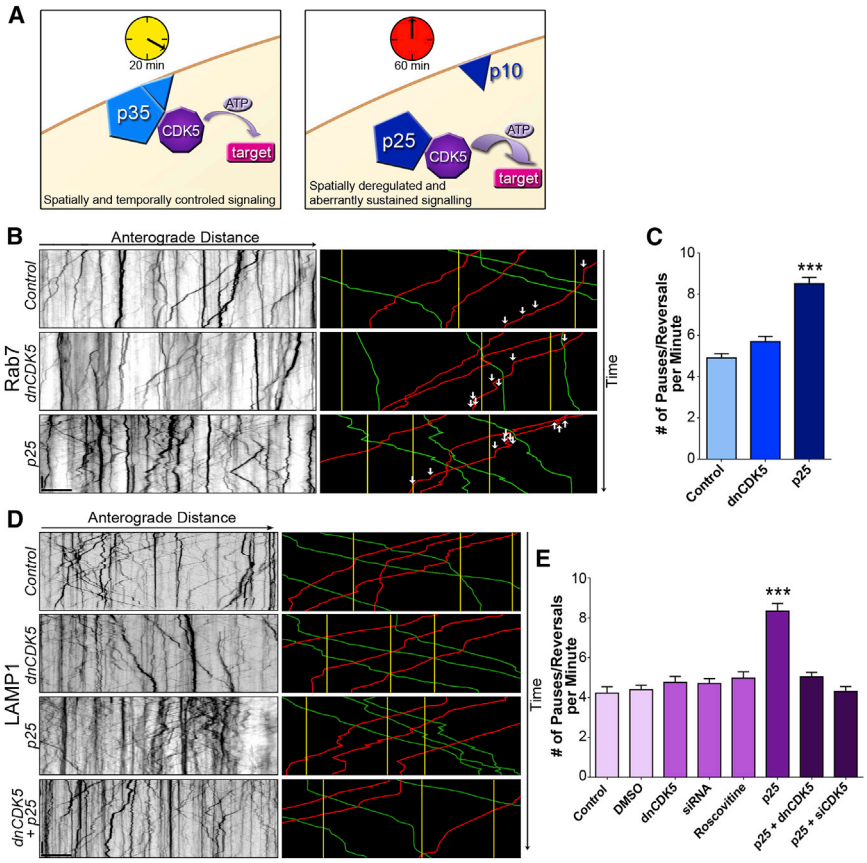

Figure 1. Activation, but Not Inhibition, of CDK5 Regulates Transport of Rab7- and LAMP1-Positive Lysosomes

(A) When bound to the endogenous membrane-bound activator p35, CDK5 activity is temporally and spatially restricted. When bound to the stress-induced activator p25, CDK5 activity is prolonged and untethered from the membrane, leading to both temporal and spatial deregulation.

(B) Kymographs of lysosomal motion in DRG neurites expressing Rab7-GFP. Representative runs are highlighted to the right of each kymograph as follows: green, anterograde; red, retrograde; and yellow, stationary. White arrows indicate individual pauses and reversals during right-most retrograde run in each.

(C) While inhibition of CDK5 had no effect on the nonprocessive motion of Rab7-tagged lysosomes, activation of CDK5 by p25 decreased processivity.

(D) Kymographs from DRG neurites transfected with LAMP1-RFP. Representative runs are highlighted to the right of each kymograph.

(E) Inhibition of CDK5 activity using multiple approaches, including expression of a dominant-negative construct (dnCDK5), depletion of endogenous CDK5 by siRNA, and treatment with the CDK5 inhibitor roscovitine, had no effect on lysosomal transport. In contrast, increasing CDK5 activity via the expression of p25 significantly increased nonprocessive events. The effects of p25 were blocked by expression of dnCDK5 or depletion of CDK5.

Scale bars represent 10 s and 10 μm. Graphs indicate means ± SEM; n = 15 neurons from at least three experiments. Differences between conditions were analyzed by one-way ANOVA with Tukey's post hoc test; ***$p < 0.001$.

as neurotrophic factors and receptors, exhibits altered axonal trafficking in the disease state (Cozzolino et al., 2012; Magrané et al., 2014; Perlson et al., 2009).

Here we investigate the role of CDK5 in the regulation of axonal transport. We find that CDK5 activity is not required to maintain constitutive transport of multiple cargos. However, elevated CDK5 activity leads to misregulation of all cargos examined. Activated CDK5 operates via the Lis1/Ndel1/dynein pathway, as the effects can be blocked by mutations that prevent the CDK5-dependent phosphorylation of Ndel1 or mutations in Lis1 that inhibit binding to dynein. Finally, we establish that the transport deficits observed in a mouse model of ALS mirror the effects induced by activation of CDK5 and can be rescued by CDK5 inhibition. Together, these observations indicate that stress-induced activation of CDK5 may contribute to the disruption of transport observed in ALS and other neurodegenerative diseases, such as Alzheimer's and Parkinson's, that exhibit dysregulated CDK5 activity.

RESULTS

CDK5 Activation, but Not Inhibition, Affects the Axonal Transport of Late Endosomes and Lysosomes

CDK5 has been reported to regulate the constitutive transport of lysotracker-positive acidic organelles (Pandey and Smith, 2011). To further investigate this possibility, we used live-cell imaging to examine the effects of changes in CDK5 activity on the motility of Rab7- and LAMP1-positive vesicles in primary dorsal root ganglia (DRG) neurons, a well-established model of axonal transport (Maday et al., 2012; Moughamian and Holzbaur, 2012; Perlson et al., 2009).

In control neurons, Rab7-positive late endosomes and lysosomes move bidirectionally along the axon, with a bias toward retrograde motility (Figure 1B). Expression of a kinase-dead dominant-negative CDK5 (dnCDK5) that binds to and sequesters p35 (Nikolic et al., 1996) did not significantly affect transport velocities (Figure S1), the ratio of motile to stationary organelles, or the number of pauses and reversals observed during processive motility. Expression of the CDK5 activator p25 also did not significantly affect the percentage of Rab7-positive lysosomes demonstrating stationary, anterograde, or retrograde motility (Table S1). However, expression of p25 led to a significant increase in the frequency of nonprocessive events interrupting rapidly moving organelles. This disruption was observed in cargos moving in both the anterograde and retrograde directions (Figures 1C and S2A).

Next we examined LAMP1-RFP, a well-characterized reporter for the motility of the late endosomal/lysosomal compartment (Moughamian and Holzbaur, 2012). Similar to our observations with Rab7-GFP, minimal changes in the bidirectional motility of

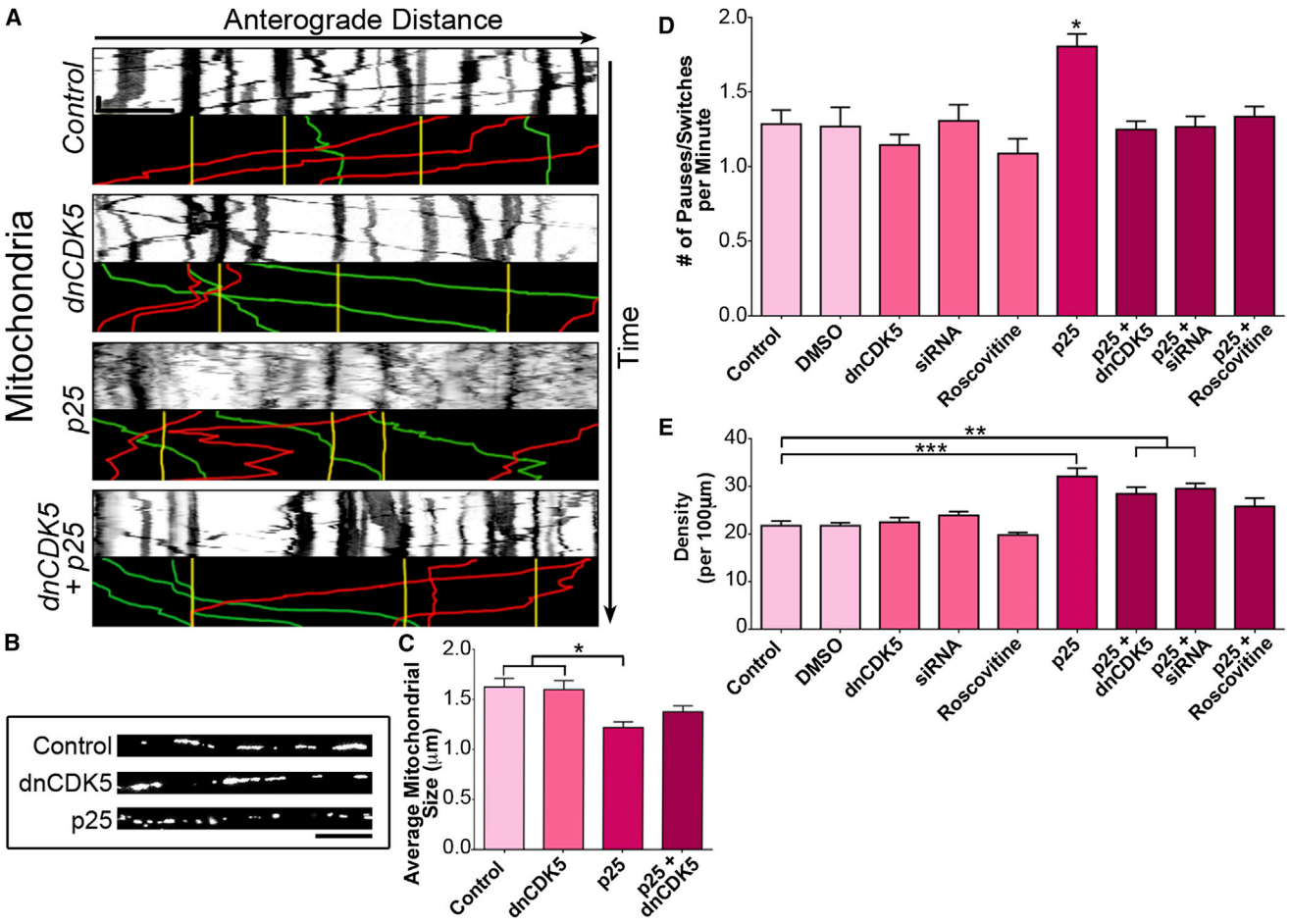

Figure 2. CDK5 Activation, but Not Inhibition, Disrupts Mitochondrial Transport

(A) Kymographs of DsRed2-mito-labeled mitochondria in DRG neurites. Representative runs are highlighted below each kymograph as follows: green, anterograde; red, retrograde; and yellow, stationary. Scale bars represent 30 s and 10 μm.

(B) Long tubular mitochondria were found along the neurites of DRG neurons in the control and dnCDK5 conditions, but they fragmented into smaller pieces upon the expression of p25.

(C) The activation of CDK5 by p25 decreased the size of mitochondria, while inhibition of CDK5 had no effect on mitochondrial length.

(D) The activation of CDK5 increased the density of mitochondria along the axon. Co-expression of p25 with either dnCDK5 or siRNA against CDK5 partially diminished the increase in mitochondrial density.

(E) The activation of CDK5 increased the nonprocessive motion of mitochondria. The effects of p25 were blocked by the inhibition of CDK5.

Graphs depict means ± SEM; n ≥ 12 neurons from at least three experiments. Values that differ significantly (one-way ANOVA with Tukey's post hoc test) are noted on graphs (*$p < 0.05$, **$p < 0.01$, ***$p < 0.001$).

LAMP1-positive organelles were observed upon expression of dnCDK5 (Figure 1D). We used two additional approaches to inhibit CDK5 activity as follows: (1) depletion of 90% of endogenous CDK5 using small interfering RNA (siRNA) (Figures S1C and S1D), and (2) pharmacological inhibition with roscovitine (Meijer et al., 1997; Zheng et al., 2007). Neither approach led to a measurable effect on axonal transport, suggesting that CDK5 activity is not required to regulate the constitutive transport of late endosomes and lysosomes along the axon.

In contrast, activation of CDK5 by p25 led to a significant increase in the frequency of nonprocessive events during directed transport of LAMP1-positive organelles, similar to the changes observed in Rab7-positive organelles. To test the specificity of this effect, we co-expressed p25 and dnCDK5 and found that the p25-induced increase in nonprocessive motility was completely blocked by CDK5 inhibition (Figures 1E and S3B). Similarly, depletion of CDK5 using siRNA blocked the alteration in motility induced by the expression of p25, supporting the conclusion that the effects of p25 are mediated by the hyperactivation of CDK5.

CDK5 Activation Disrupts Mitochondria Transport

Next, we examined mitochondrial motility using the marker DsRed2-mito, which labels both tubular and vesicular mitochondria in the axon (Figure 2B). Robust bidirectional motility of large and small mitochondria was observed (Figure 2A; Table S1). Similar to our observations for late endosomes/lysosomes, expression of dnCDK5, depletion of endogenous CDK5 by

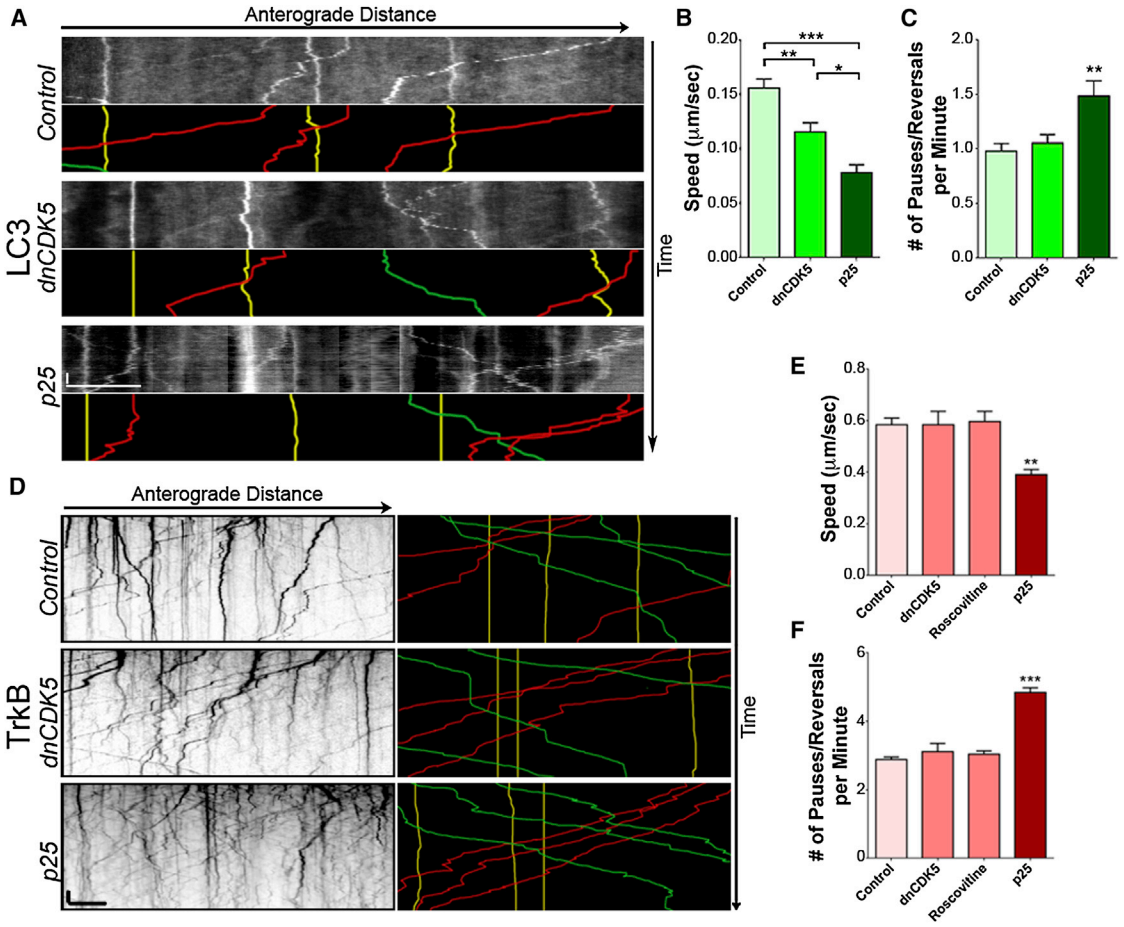

Figure 3. Activation of CDK5 Decreases the Motility of Retrograde-Directed Cargos

(A) Kymographs of autophagosomes in DRG neurites from mice expressing GFP-LC3. Representative runs are highlighted below each kymograph as follows: green, anterograde; red, retrograde; and yellow, stationary.

(B) Ensemble speeds of autophagosomes decreased with increased CDK5 activity.

(C) The activation of CDK5 increased the nonprocessive motion of retrograde-directed LC3 cargo.

(D) Kymographs of TrkB motion in DRG neurites transfected with TrkB-mRFP. Representative runs are highlighted to the right of each kymograph.

(E) Speed of actively transported TrkB cargo decreased with increased CDK5.

(F) The inhibition of CDK5 activity by dnCDK5 or the chemical inhibitor roscovitine had no effect on processivity of TrkB. In contrast, activation of CDK5 increased nonprocessive motion of TrkB cargo.

Scale bars represent 10 s and 10 μm. Graphs depict means ± SEM; n ≥ 15 neurons from at least three experiments. Values that differ significantly (one-way ANOVA with Tukey's post hoc test) are noted on graphs (*$p < 0.05$, **$p < 0.01$, ***$p < 0.001$).

siRNA, or chemical inhibition had no effect on mitochondrial motility. However, p25-induced activation of CDK5 increased the number of nonprocessive events exhibited by actively moving mitochondria. Again, the increase in oscillatory motion induced by p25 expression was reduced by co-expression of dnCDK5, depletion of CDK5 by siRNA, or treatment with the chemical inhibitor roscovitine (Figures 2D and S2B), indicating the specificity of the observed effects.

p25 expression also resulted in increased fragmentation of mitochondria (Figures 2B and 2C) as well as an increase in mitochondrial density along the axon, as previously noted (Meuer et al., 2007). Neurons exposed to diminished levels of CDK5 activity (dnCDK5, siRNA to CDK5, roscovitine) did not exhibit changes in mitochondrial density or fragmentation (Figure 2E). While co-expression of dnCDK5 or depletion of endogenous CDK5 by siRNA was not sufficient to block these effects, roscovitine treatment was sufficient to rescue the effects on mitochondrial density induced by p25.

Perturbation of CDK5 Activity Strongly Disrupts Transport of Retrograde-Biased Cargos

Both lysosomes and mitochondria are bidirectional cargo; thus, their motility results from the coordinated activities of both dynein and kinesins (Maday et al., 2014). To more directly examine the effects of CDK5 on dynein-driven transport, we imaged GFP-LC3-positive autophagosomes (Klionsky et al., 2012; Maday et al., 2012), which move in a robust retrograde manner along the axon (Figure 3A). Autophagosome motility

was decreased with any modulation of CDK5 activity (Table S1), although p25 expression induced the most pronounced effects. The decrease in motility and the increase in oscillatory events led to a striking decrease in the ensemble speed of retrograde-directed autophagosomes induced by changes in CDK5 expression (Figure 3B).

The number of pauses and reversals during autophagosome transport was measured in neurons overexpressing either dnCDK5 or p25. Autophagosomes displayed an increase in nonprocessive events when CDK5 activity was increased via p25 expression (Figure 3C). Thus, autophagosomes, lysosomes, and mitochondria all exhibited increased pauses and switches upon CDK5 activation by p25. In contrast, reduction of CDK5 activity had no significant effect on the motility of lysosomes or mitochondria, but did reduce the ensemble speed of autophagosomes.

TrkB, the receptor for neurotrophic factor BDNF, moves bidirectionally in neurons, with a bias toward retrograde motility (Table S1). Reduction of CDK5 activity either by the expression of dnCDK5 or roscovitine treatment had no effect on the transport of mRFP-TrkB-positive endosomes. In contrast, p25-induced activation of CDK5 led to oscillatory movement of TrkB, similar to the effects observed for other cargos (Figures 3D and 3F); we also noted a decrease in the peak velocity of TrkB transport (Figure 3E).

Active CDK5 Promotes Dynein Binding to Microtubules

Together, these observations indicate that increased CDK5 activity affects the transport of multiple axonal cargos, with the most striking effects observed for retrograde-directed cargos. This suggests that the retrograde motor dynein may be the target of CDK5 activity. The binding of ATP to dynein induces the release of the motor from the microtubule by inducing a conformational change in dynein's linker domain; the dynein-binding protein Lis1 modulates this conformational change, enhancing the strongly bound state (Huang et al., 2012). Ndel1, a known phosphorylation target of CDK5, enhances the binding of Lis1 to dynein (McKenney et al., 2010; Niethammer et al., 2000). We hypothesized that the CDK5-dependent phosphorylation of Ndel1 would promote the formation of a more stable Lis1/Ndel1/dynein complex and thus induce a sustained interaction of dynein with the microtubule. For organelles trafficking along the axon, this would be predicted to lead to an increase in pauses and reversals upon activation of CDK5 by p25.

To determine whether the binding of dynein to microtubules is enhanced by activated CDK5, a microtubule-binding assay was performed using HeLa cell lysates expressing CDK5 or co-expressing CDK5 and p25 (Figure 4A). Co-expression of CDK5 and p25 significantly enhanced the binding of dynein to microtubules in the presence of ATP as compared to CDK5 alone (Figure 4B).

A high-resolution in vitro assay was used to determine if CDK5 affects dynein motility by favoring increased attachment to the microtubule. Lysates from HeLa cells stably expressing GFP-tagged dynein heavy chain (DHC-GFP) (Kiyomitsu and Cheeseman, 2012) and transfected with CDK5, or both CDK5 and p25, were depleted of ATP and perfused into a flow chamber with rhodamine-tagged microtubules fixed to glass coverslips (Figure 4C). Total internal reflection fluorescence (TIRF) microscopy was used to image individual dynein motors bound to microtubules. Images of the same microtubules were captured before and after the addition of 10 mM Mg-ATP (Figure 4D). Following the addition of ATP, we observed a release of dynein from the microtubule in lysates expressing CDK5. In contrast, the addition of ATP to lysates expressing CDK5 and p25 did not significantly alter dynein binding from pre-ATP levels (Figures 4E and 4F). Together these results demonstrate that activated CDK5 enhances the binding of dynein to microtubules, even in the presence of saturating ATP.

CDK5 Controls Dynein Motion via a Lis1/Ndel1-Dependent Mechanism

Our in vitro experiments indicate that activated CDK5 is sufficient to induce sustained binding of dynein to microtubules, but CDK5 does not directly phosphorylate dynein (Hallows et al., 2003). One well-characterized target of CDK5-dependent phosphorylation is Ndel1 (Pandey and Smith, 2011). A 2:2 complex of Lis1 and Ndel1 binds the dynein motor (Figure 5A) and phosphorylation of Ndel1 enhances this binding (Zyłkiewicz et al., 2011). Ndel1 contains five CDK5 phosphorylation sites as follows: S198, T219, S231, S242, and T245 (Figure 5B; Niethammer et al., 2000); mutating these five residues to alanine (Ndel1 mut) blocks the CDK5-dependent phosphorylation of Ndel1 (Hebbar et al., 2008).

To determine whether phosphorylation of Ndel1 by CDK5 is required to induce the observed effects on dynein motility, we expressed either wild-type Ndel1 or the unphosphorylatable Ndel1 mutant along with LAMP1-RFP. Overexpression of either Ndel1 construct did not affect the speed or extent of motility; co-expression of dnCDK5 also did not disrupt lysosomal motility in the presence of either Ndel1 construct (Figure 5D, middle). While p25 expression increased the number of oscillatory events interrupting the transport of lysosomes in the presence of wild-type Ndel1, expression of unphosphorylatable Ndel1 significantly reduced the defects in lysosomal motility caused by p25 expression (Figure 5E), supporting our hypothesis that phosphorylation of Ndel1 regulates CDK5-dependent changes in transport.

Next, we asked whether the p25-induced changes in lysosomal transport were Lis1 dependent. Lis1 contains two regions essential for binding dynein. Mutation of K147 (Figure 5C) disrupts the binding of Lis1 to dynein, but not to Ndel1 (Mesngon et al., 2006). We found that expression of the Lis1 K147A mutant reduced both anterograde and retrograde transport of lysosomes, regardless of the activity level of CDK5 (Figure 5D, far right). This reduction was accompanied by an increase in stationary lysosomes but did not change lysosomal density. The same changes were not observed with overexpression of wild-type Lis1 (Figure S4). Despite the overall decrease in motility, some lysosomes continued to exhibit robust movement in the presence of the Lis1 mutant, allowing for analysis of pauses and directional switches. Among the motile lysosomes, expression of the Lis1 mutant reduced the magnitude of the p25-induced increase in nonprocessive events. Although LAMP1-positive lysosomes exhibited a slight increase in the number of nonprocessive events when p25 was expressed in the presence of Lis1 K147A, this increase was minimal in comparison to the

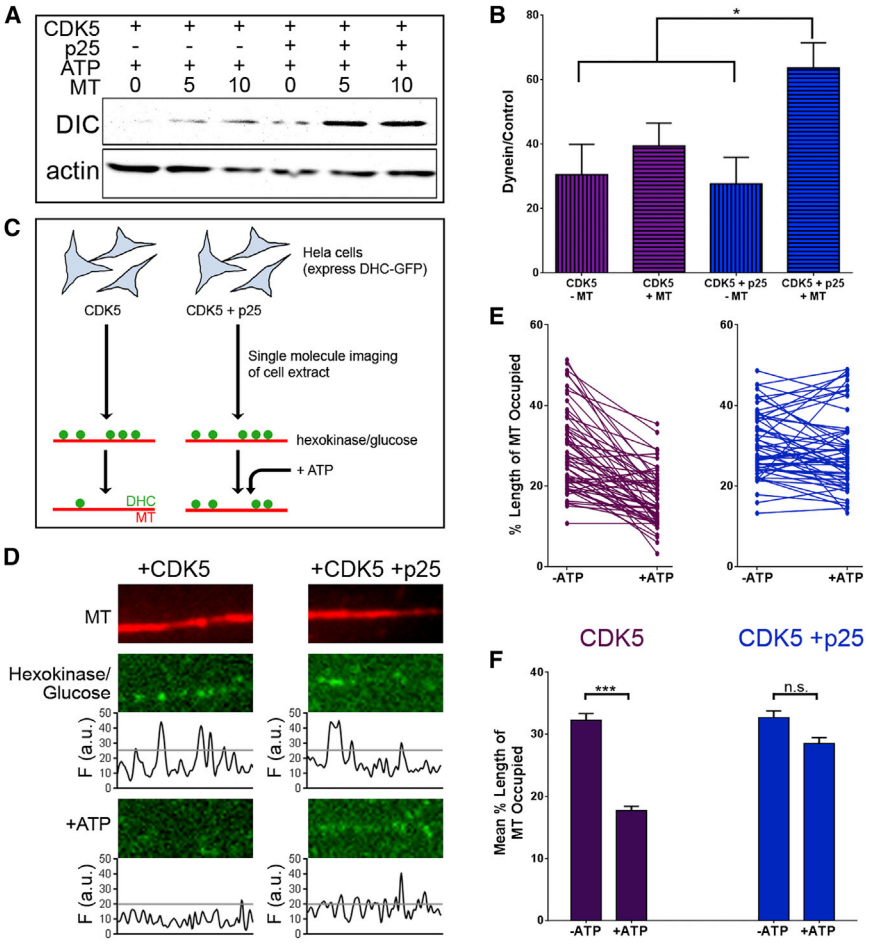

Figure 4. Activated CDK5 Enhances Binding of Dynein to Microtubules In Vitro

(A) Extracts of HeLa cells expressing CDK5 or CDK5 and p25 were exposed to 0, 5, or 10 μM taxol-stabilized microtubules in the presence of 10 mM MgATP. Microtubule pellets were probed for the binding of dynein intermediate chain (DIC).

(B) The addition of p25 increased dynein binding to microtubules relative to CDK5 alone (means ± SEM; n = 4 experiments).

(C) Schematic of the TIRF assay used to assess dynein binding to the microtubule. HeLa cells expressing DHC-GFP and endogenous levels of Lis1 and Ndel1 were transfected with CDK5 or CDK5 and p25. Lysates from transfected cells were perfused into a flow chamber with rhodamine-tagged microtubules fixed to a glass coverslip in the presence of hexokinase and glucose to induce the rigor-bound state of dynein. ATP was then added to the chambers to induce the release of dynein from the microtubule.

(D) TIRF images of a microtubule (top) and attached dynein motors. Depletion of ATP (hexokinase/glucose) caused decoration of microtubules with rigor-bound dynein (middle). Addition of 10 mM MgATP in the absence of activated CDK5 induced dynein release from the microtubule (bottom left). In the presence of activated CDK5, ATP-induced dissociation of dynein from the microtubules was significantly inhibited (bottom right).

(E) The addition of ATP induced the release of dynein from microtubules in the presence of inactive CDK5. Individual lines on the graph indicate the change in dynein binding along a single microtubule before (−ATP) to after (+ATP) the addition of 10 mM ATP. Data from 54 microtubules and three experiments.

(F) The mean percentage of microtubule decorated by dynein decreased significantly when CDK5 was inactive, but not when active CDK5 was present (means; n ≥ 108 microtubules from seven chambers over three experiments). *p < 0.05, ***p < 0.001, n.s. indicates p > 0.05 (two-way ANOVA with Tukey's post hoc test).

increase observed upon expression of p25 in the absence of the Lis1 mutant (Figure 5F).

Previous work has shown that depletion of Lis1 causes dramatic inhibition of lysosomal motility (Moughamian et al., 2013), consistent with our finding that decreasing the affinity of Lis1 for dynein reduced the number of anterograde- and retrograde-directed lysosomes (Figure 5G). Co-expression of the dnCDK5 construct with mutant Lis1 resulted in the strongest reduction in motility.

We also examined the effects of the Ndel1 mutant on autophagosome transport, as the pronounced retrograde motion of these organelles is dynein mediated (Maday et al., 2012). As observed for lysosomes, GFP-LC3-labeled autophagosomes displayed minimal changes in transport when either wild-type or unphosphorylatable Ndel1 was expressed, at either unmodified or diminished levels of CDK5 activity (Figure 5H). Hyperactivation of CDK5 by p25 led to a significant disruption of transport, as observed by an increase in oscillatory events when wild-type Ndel1 was overexpressed. However, expression of the mutant form of Ndel1 was sufficient to block the p25-induced disruption of autophagosome transport (Figures 5H and 5I).

Autophagosomes, like lysosomes, displayed diminished overall transport in the presence of mutant Lis1, independent of any perturbations in CDK5 activity (Figures 5H and 5K). This observation is consistent with a key role for Lis1 in dynein-mediated organelle transport (Moughamian et al., 2013). However, we did not observe a p25-induced increase in nonprocessive events in the few motile puncta in the presence of mutant Lis1 (Figure 5J), supporting the model that both Ndel1 and Lis1 are necessary downstream effectors of CDK5/p25-induced nonprocessive motility.

SOD1^{G93A} Mice Exhibit Dysregulated CDK5 Activity

Next, we sought to investigate a possible role for elevated CDK5 activity in driving the pathogenic changes in axonal transport observed in models of ALS using the well-characterized SOD1^{G93A} mouse. Elevated p25 expression and increased CDK5 activity have been identified previously in the SOD1^{G37R} mouse line (Nguyen et al., 2001). To determine whether there is a similar activation of CDK5 in the SOD1^{G93A} mouse, high-speed supernatant fractions from spinal cords of 90- to 100-day-old SOD1^{G93A} mice and wild-type littermate controls were probed for the expression of p35 and p25 using an antibody that recognizes both proteins

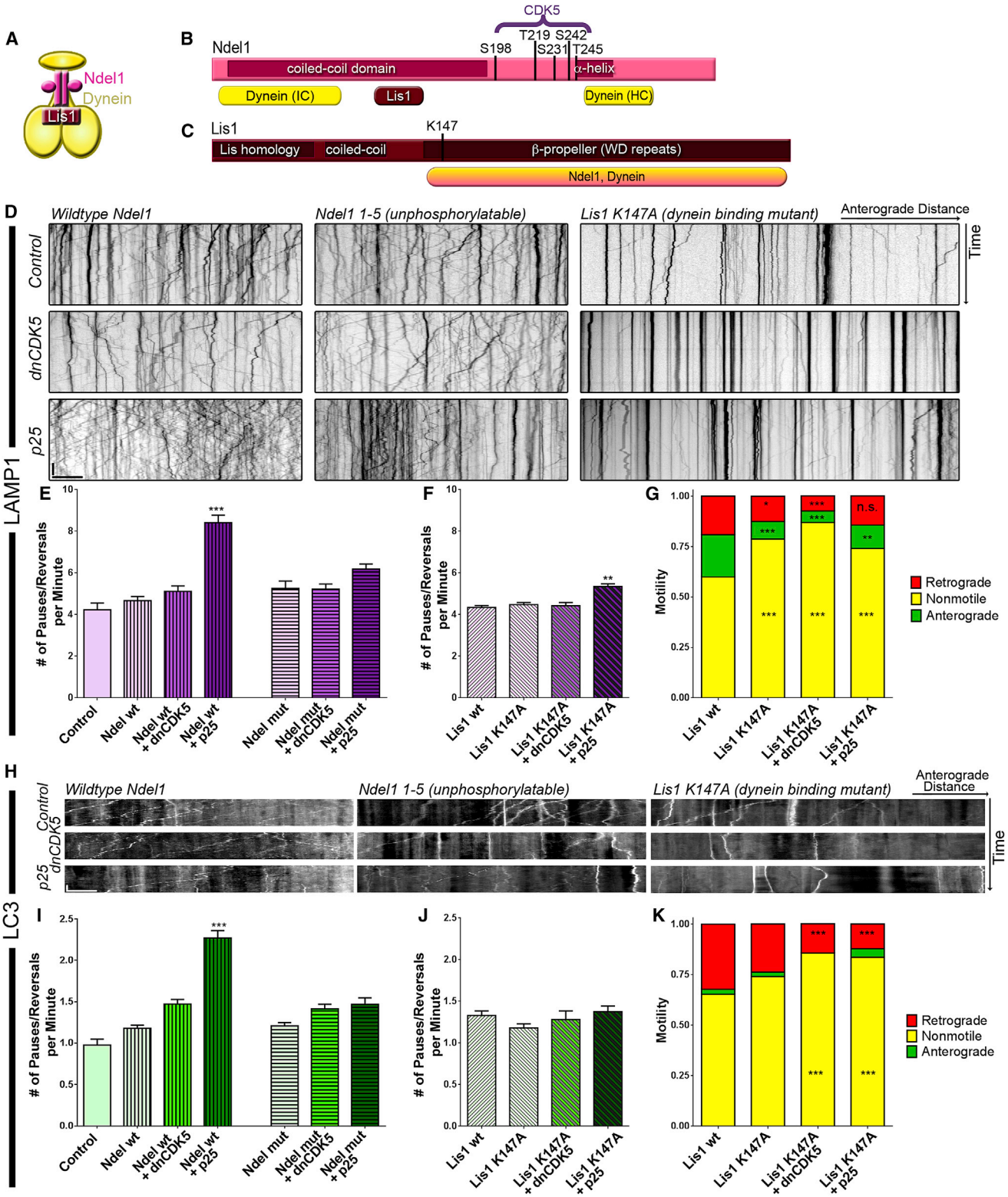

Figure 5. Nonprocessive Motion of Degradative Cargo Induced by CDK5 Activation Depends on a Lis1/Ndel1/Dynein Mechanism

(A) Phosphorylated Ndel1 enhances Lis1 binding to dynein (Zyłkiewicz et al., 2011).

(B) Ndel1 contains five CDK5 phosphorylation sites. All five sites were mutated to Niethammer et al. (2000). Ndel1 also contains two dynein-binding regions and a Lis1-binding region, as well as a coiled-coil domain and an α-helical domain.

(legend continued on next page)

(Figure 6A). Quantitative analysis revealed a greater than 2-fold increase in the p25/p35 ratio in the high-speed fraction from spinal cord lysates from SOD1^{G93A} mice (Figure 6C), indicating activation of CDK5 in this model. We also probed spinal cord lysates from SOD1^{G93A} mice and wild-type littermates with a phospho-specific antibody to the T219 residue of Ndel1 (Figure 6B). Animals expressing mutant SOD1 exhibited almost double the level of phosphorylated Ndel1 compared to wild-type animals (Figure 6D).

Inhibition of CDK5 Rescues Disrupted TrkB Transport in SOD1^{G93A} Neurons

Defects in the retrograde transport of neurotrophic factors have been proposed to contribute to the neuronal death characteristic of ALS (Henriques et al., 2010). Processive motility of signaling endosomes in neurons from SOD1^{G93A} mice was shown to be disrupted by frequent pauses and switches (Perlson et al., 2009); in vivo analysis of transport in this model also showed enhanced pausing of cargos along the axon (Bilsland et al., 2010). The similarity of these observations to the nonprocessive motility induced by p25 expression led us to ask whether the hyperactivation of CDK5 might contribute to the observed deficits in axonal transport.

We assessed the effects of CDK5 inhibition on signaling endosome motility in DRG neurons cultured from 90- to 100-day-old SOD1^{G93A} mice. We observed an increase in the oscillatory motion of mRFP-tagged TrkB when compared to age-matched controls (Figure 6E). Importantly, the oscillatory motion observed in SOD1^{G93A} neurons was diminished in the presence of the CDK5 inhibitor roscovitine, suggesting that increased CDK5 activity was responsible for the abnormal motility (Figure 6F). TrkB was transported more slowly in neurons expressing mutant SOD1; this effect also was rescued by roscovitine treatment (Figure 6G). Parallel experiments using dnCDK5 to inhibit CDK5 activity did not completely restore motility, likely due to lower expression levels of the transfected construct in SOD1^{G93A} neurons (data not shown). However, our observations with roscovitine suggest that hyperactive CDK5 contributes to the disruption in transport observed in this ALS model, and that CDK5 inhibition can mitigate the effects of mutant SOD1 on axonal transport.

DISCUSSION

Here we found that inhibition of CDK5 does not significantly affect the axonal transport of numerous cargos, including late endosomes, lysosomes, and mitochondria. The following three CDK5 inhibitors were assessed: a dnCDK5 construct, a chemical inhibitor (roscovitine), and depletion of endogenous CDK5 by siRNA. All three failed to affect the processivity, motility, or speed of bidirectional cargo. While prior work reported that expression of dnCDK5 induced a complete block in the transport of lysotracker-positive organelles (Pandey and Smith, 2011), these experiments were conducted using a model in which sciatic nerve crush was performed prior to DRG isolation; this procedure may affect downstream regulatory mechanisms. As we found that expression of dnCDK5, depletion of endogenous CDK5, or chemical inhibition of CDK5 did not significantly affect the motility of lysosomes in wild-type DRG neurons, we conclude that CDK5 does not play a significant role in the regulation of constitutive axonal transport in this model.

Although reduction of CDK5 activity had little effect on axonal transport in our experiments, increasing CDK5 activity significantly altered the dynamics of cargo transport. Expression of the CDK5 activator p25 increased the likelihood that late endosomes/lysosomes or mitochondria would pause or reverse direction during periods of directed motion. Despite the increase in nonprocessive events, these bidirectional cargos did not display net changes in speed (Figures S1E and S2A). For lysosomes, the increased frequency of non-motile events was matched by a decrease in the duration of each event (Figures S1G and S1H). In the context of increased CDK5 activity, pauses were shorter and directional changes covered less distance before resuming the initial direction of motion.

Increased CDK5 activity more significantly altered the transport of TrkB-positive signaling endosomes and autophagosomes; these unidirectional cargos exhibited reductions in peak speed when CDK5 was aberrantly activated, along with an increase in nonprocessive events. As retrograde cargos rely primarily on dynein for motility, we propose that alterations in the mechanochemistry of dynein more profoundly affect their speeds. In contrast, bidirectional cargos, such as lysosomes

(C) Lis1 contains a Lis-homology domain (LH) for dimerization, as well as a coiled-coil domain, and a β-propeller domain that binds to dynein and Ndel1. A mutation in K147 disrupts binding to dynein (Mesngon et al., 2006).
(D) Kymographs of lysosomal motion in neurons transfected with wild-type Ndel1, mutant Ndel1 unphosphorylatable by CDK5, and a Lis1 K147A mutant that cannot bind dynein (Mesngon et al., 2006). Lysosomes were labeled with LAMP1-RFP.
(E) The increase in nonprocessive events induced by p25 was blocked by the expression of non-phosphorylatable Ndel1. Vertical stripes indicate transfection with wild-type Ndel1; horizontal stripes indicate transfection with unphosphorylatable Ndel1. Only $p < 0.0001$ are noted.
(F) The effects of p25 expression on processivity of lysosomal transport were less pronounced in the setting of the Lis1 K147A mutant.
(G) Expression of the Lis1 K147A mutation reduced the number of anterograde- and retrograde-directed lysosomes while increasing the percentage of stationary (total run lengths <10 μm) lysosomes compared to overexpression of a Lis1 wild-type construct.
(H) Kymographs of autophagosomes labeled with LC3-GFP in the presence of wild-type or mutant Ndel1 and mutant Lis1 are shown.
(I) The number of nonprocessive events in autophagosome transport was reduced in the absence of phosphorylatable Ndel1. Vertical stripes indicate transfection with wild-type Ndel1; horizontal stripes indicate transfection with unphosphorylatable Ndel1. Only $p < 0.0001$ are noted.
(J) Variations in CDK5 activity had no effect on autophagosome transport in cells expressing the Lis1 mutant.
(K) Expression of the Lis1 K147A mutation reduced the number of retrograde-directed autophagosomes while increasing the percentage of stationary autophagosomes.
Scale bars represent 10 s and 10 μm. Graphs depict means ± SEM; $n \geq 16$ neurons from at least three experiments. Values that differ significantly (one-way ANOVA with Tukey's post hoc test, E, F, I, and J, or two-way ANOVA with Tukey's post hoc test, G and K) are noted on graphs (*$p < 0.05$, **$p < 0.01$, ***$p < 0.001$); n.s. or no asterisks indicates $p > 0.05$.

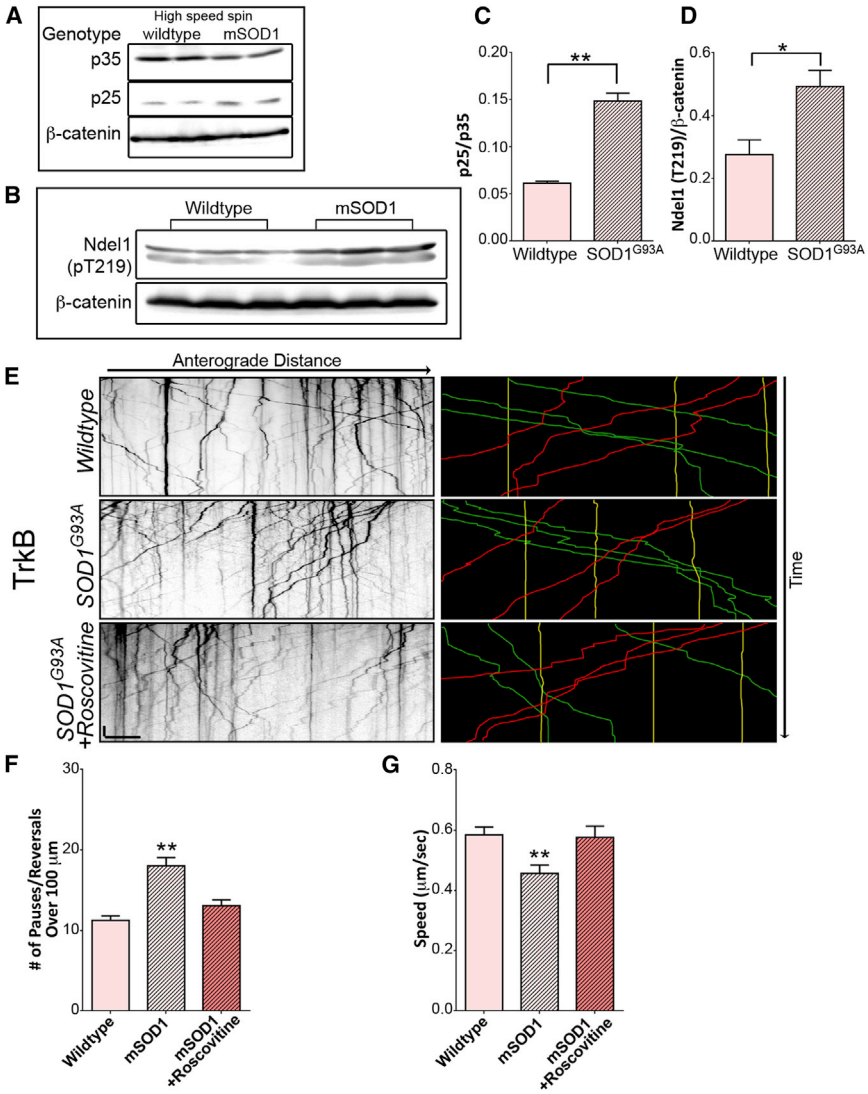

Figure 6. SOD1 Mutant Mice Have Deregulated CDK5 Activation Resulting in Transport Disruption, Which Can Be Rescued by Reducing CDK5 Activity

(A) Western blots of low-speed and high-speed extracts of spinal cord from SOD1^{G93A} and age-matched wild-type mice with an antibody recognizing both p35 and p25. Blots also were stained for β-catenin.

(B) Western blots of spinal cord extracts from SOD1^{G93A} and wild-type littermate mice with a phospho-T219-specific antibody to Ndel1. Blots also were stained for β-catenin.

(C) An increase in p25/p35 ratio was found in high-speed extracts from SOD1^{G93A} mice as compared with wild-type littermate mice (means ± SEM; n = 4 mice).

(D) Spinal cords from SOD1^{G93A} mice expressed higher levels of Ndel1 phosphorylation at CDK5 site T219 than wild-type littermate animals (means ± SEM; n = 6 mice).

(E) Kymographs of TrkB motion in DRG neurites from 90- to 100-day-old SOD1^{G93A} mice transfected with TrkB-mRFP in the absence and presence of roscovitine. Representative runs are highlighted to the right of each kymograph as follows: green, anterograde; red, retrograde; and yellow, stationary.

(F) Expression of mutant SOD1 increased nonprocessive motion of TrkB cargo. Reducing CDK5 activity in SOD1^{G93A} neurons using roscovitine rescued the observed effects on transport (mean ± SEM; n ≥ 18 neurons from three experiments).

(G) Speed of actively transported TrkB cargo decreased significantly in SOD1^{G93A} mice (means ± SEM; n ≥ 18 neurons from three experiments).

Scale bars represent 10 s and 10 μm. Values that differ significantly (Student's t test, C and D, one-way ANOVA with Tukey's post hoc test, F and G) are noted on graphs (*p < 0.05, **p < 0.01, ***p < 0.001).

and mitochondria, have both dynein and kinesin motors bound to them (Fu and Holzbaur, 2014); we hypothesize that the powerful kinesin motors bound to these cargos may effectively overcome the pausing induced by Lis1-bound dynein motors.

In addition to decreasing processive motion of cargo, increasing CDK5 activity via p25 also increased cargo density in the mid-axon. This was most notable for mitochondria, which previously have been determined to undergo fission in the presence of elevated CDK5 activity (Meuer et al., 2007). Lysosomes, autophagosomes, and signaling endosomes also exhibited increased density upon CDK5 activation (Figures S1F and S3), but no parallel changes in organelle size were observed. It is possible that the increased density is due to an increase in cargo trafficking to the axons, as studies in *C. elegans* have implicated CDK5 in axonal-dendritic cargo sorting (Goodwin et al., 2012; Ou et al., 2010). In contrast, reducing CDK5 activity levels did not alter the density of cargo in the mid-axon for any of the cargos examined.

The generalized response to increased CDK5 activity implicates a common regulatory mechanism. Previous studies identified Ndel1 as a phosphorylation target of CDK5 (Niethammer et al., 2000), leading us to hypothesize that CDK5 could affect transport of a wide range of cargo via the Lis1/Ndel1/dynein complex. Consistent with this, we found that blocking the CDK5-dependent phosphorylation of Ndel1 significantly reduced the p25-induced increase in nonprocessive motility; expression of a dynein-binding mutant of Lis1 also blocked the effects of CDK5 activation.

The observations reported here argue that CDK5 is not involved in the regulation of constitutive axonal transport along the axon. Instead, our results point to a model in which cellular stress leads to the spatially and temporally unregulated activation of CDK and the hyperphosphorylation of Ndel1. This phosphorylation frees Ndel1 from auto-inhibition, promoting the formation of a Lis1/Ndel1/dynein complex (Bradshaw et al., 2013; Zyłkiewicz et al., 2011). This complex acts as a clutch (Huang

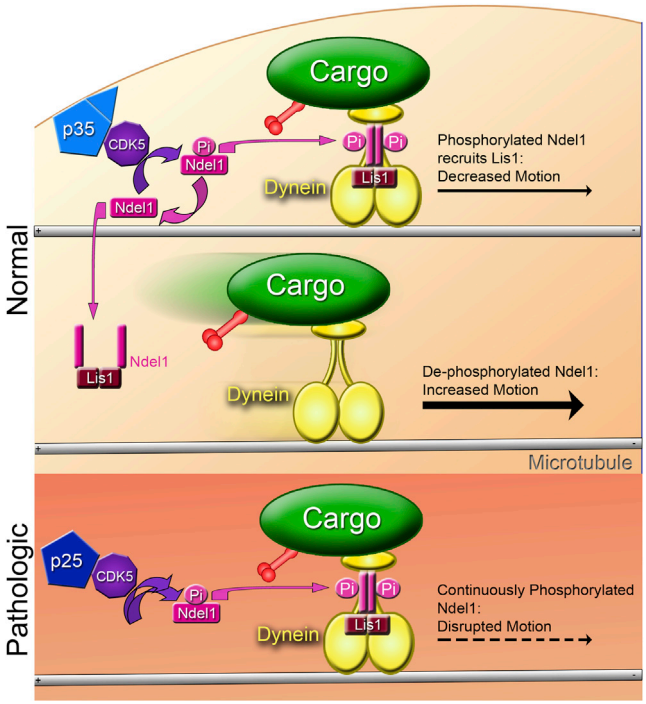

Figure 7. Model for the CDK5-Dependent Regulation of Transport through Ndel1, Lis1, and Dynein

Cargo is actively transported in the retrograde direction by dynein or the anterograde direction by kinesin. CDK5 is activated in healthy cells by membrane-bound p35 in a spatially and temporally specific manner. (Top) Ndel1, phosphorylated by activated CDK5, recruits Lis1 to dynein, leading to a sustained interaction of dynein with the microtubule. This causes increased pausing during transport. (Middle) Dephosphorylation of Ndel1 causes the Lis1/Ndel1 complex to release from dynein. Dynein pauses less often without the Lis/Ndel clutch. However, without Lis1 and Ndel1 to hold dynein to the microtubule, dynein is more likely to disengage when encountering an obstacle. (Bottom) In the pathologic state, p35 is cleaved into p25, which causes prolonged and mislocalized activation of CDK5. This, in turn, causes increased phosphorylation of Ndel1, leading to strong recruitment of Lis1 to dynein and subsequent disruption of transport.

et al., 2012) that interrupts processive motility along the axon (Figure 7, top). In contrast, dephosphorylated and auto-inhibited Ndel1 cannot bind dynein. Without the Lis1/Ndel1 complex bound, dynein processes easily, but is prone to detach from the microtubule, as the clutch function of Lis1 and Ndel1 is not available to block dissociation when an obstacle is encountered (Figure 7, middle; Huang et al., 2012). As this mechanism is dynein dependent, organelles that primarily move retrogradely are more strongly affected by changes in CDK5 levels.

In stressed neurons, both the prolonged activation and the mislocalization of CDK5 induced by p25 causes Ndel1 to remain consistently phosphorylated, thus enhancing the formation of the Lis1/Ndel1/dynein complex and causing an increase in the frequency of interrupted runs of motion (Figure 7, bottom). As a result, enhanced phosphorylation of Ndel1 is pathological. Prolonging the engagement of dynein with the microtubule through hyperphosphorylation of Ndel1 also would be likely to transiently stall kinesin-driven transport, as both dynein and kinesin are bound to most cargos actively transported along the axon (Fu and Holzbaur, 2014). However, kinesin is more powerful than dynein and more likely to win a sustained tug-of-war (Hancock, 2014), potentially explaining why cargos with active kinesin motors exhibit less disruption of motility than what was observed for predominantly retrograde cargos (Figure S1G).

The disruption of transport induced by CDK5 activation is reminiscent of previous observations demonstrating enhanced pausing and switches of cargos moving along axons of neurons from SOD1^{G93A} mice (Bilsland et al., 2010; Perlson et al., 2009). Further, both p25 levels and CDK5 activity are known to be elevated in the SOD1^{G37R} mouse line (Nguyen et al., 2001). Here we confirmed this observation in the SOD1^{G93A} model and tested the effects of reducing CDK5 activity. Inhibition of CDK5 rescued the transport defect observed in neurons from SOD1^{G93A} mice and corrected the mitochondrial fragmentation phenotype (Figure S5), suggesting that treatment with CDK5 inhibitors may restore deficits in axonal transport in affected neurons in ALS. CDK5 inhibitors have been shown to mitigate neurological damage in stroke models (Menn et al., 2010); a similar therapy may be of value in the treatment of patients with ALS.

Taken together, this study highlights the differences in CDK5-dependent regulation of transport between healthy and stressed neurons. In healthy cells, CDK5 has minimal effect on cargo transport. However, when hyperactivated by p25, mislocalized CDK5 disrupts transport by increasing the number of nonprocessive events for cargos including lysosomes, mitochondria, autophagosomes, and signaling endosomes. Further, we identify a Lis1/Ndel1-dependent mechanism by which pathological activation of CDK5 leads to the misregulation of axonal transport. As elevated CDK5 levels seen in neurons from multiple disease models correlate with defects in axonal transport, these transport defects potentially may be ameliorated by therapeutics targeted to modulation of CDK5 activation.

EXPERIMENTAL PROCEDURES

Reagents, extraction of spinal cord lysates, and CDK5 depletion are described in detail in the Supplemental Experimental Procedures.

Live-Cell Imaging

DRG neurons were isolated from mice according to Perlson et al. (2009); all animal protocols received prior approval from the University of Pennsylvania Institutional Animal Care and Use Committee. Neurons were maintained in F-12 media (Invitrogen) with 10% heat-inactivated fetal bovine serum, 2 mM L-glutamine, 100 U/ml penicillin, and 100 μg/ml streptomycin. For live-cell analysis, DRG neurons were plated on glass-bottom dishes (World Precision Instruments) and cultured for 2 days at 37°C in a 5% CO_2 incubator. Before plating, neurons were transfected with 0.5–0.7 μg plasmid DNA or 20–60 pM siRNA as noted, using a Nucleofector (Lonza) according to the manufacturer's specifications. Then 20 mM roscovitine (Cell Signaling Technology) or DMSO was added as noted 24 hr prior to imaging. Imaging was performed in low-fluorescence nutrient medium (Hibernate A, BrainBits) with 2% B27 and 2 mM GlutaMAX on an inverted epifluorescence microscope (DMI6000B, Leica Camera AG) using an Apochromat 63×, 1.4 NA oil immersion objective (Leica Camera AG) in an environmental chamber at 37°C. Digital images were acquired with an ORCA-R2 (Hamamatsu) using LAS-AF software (Leica Camera AG). Images were taken every 3 s for a total of 3 min for GFP-LC3 and DsRed2-mito, every 368 ms for a total of 1.06 min

for GFP-Rab7 and LAMP1-RFP, and every 500 ms for a total of 2 min for mRFP-TrkB.

Image Analysis

Kymographs were generated using MetaMorph. Only healthy neurons were included, as defined by displaying >10% motile puncta (traveling a net distance of ≥10 μm) for LAMP1-RFP, GFP-Rab7, and mRFP-TrkB or >5% motile DsRed2-mito puncta. An exception was made for neurons expressing Lis1 K147A, where ≥5% motility of LAMP1-RFP puncta was required for inclusion. The total number of vesicles was determined and normalized by kymograph length; mitochondrial size was determined by line scan. Fluorescent puncta were tracked from the beginning to the end of the kymograph to characterize motion as anterograde (≥10 μm), retrograde (≥10 μm), or nonmotile (<10 μm). To focus specifically on the interruption of highly processive motility, three puncta per kymograph that traveled the farthest distance over the imaging sequence, in either the anterograde or retrograde direction, were tracked manually using ImageJ and assessed for total run length, run time, and number of pauses and reversals. A pause was defined as single or consecutive instantaneous velocities of <0.067 μm/s, the resolution of our system. A reversal was defined as a displacement of ≥1.5 μm in the direction opposite to net cargo displacement. Peak speed was determined using the fastest three anterograde and retrograde cargo per kymograph. Ensemble speed was determined using all available vesicles, stationary or moving. All movies were recorded in the mid-axon, >70 μm from both the axon tip and cell body.

TIRF Assay for Microtubule Binding

HeLa cells expressing GFP-DHC (Kiyomitsu and Cheeseman, 2012) (A. Hyman, Max Planck Institute) were transiently transfected with Fugene 6 (Roche) and harvested 20–24 hr post-transfection. For microtubule binding assays, transfected HeLa cells were lysed in 40 mM HEPES, 1 mM EDTA, 120 mM NaCl, 0.1% Triton X-100, and 1 mM MgATP supplemented with protease inhibitors (1 mM PMSF, 0.01 mg/ml TAME, 0.01 mg/ml leupeptin, and 0.001 mg/ml pepstatin-A). Lysates were clarified by centrifugation at 1,000 × *g* and then at 100,000 × *g*. Clarified lysates were diluted in P12 buffer (12 mM PIPES, 1 mM EGTA, and 2 mM $MgCl_2$ [pH 6.8]) immediately before perfusion into the flow chamber. For a 70%–80% confluent 10-cm plate, cells were lysed in 100 μl lysis buffer, which was then diluted 1:20 or 1:50 for single-molecule imaging. Anti-tubulin antibody (Sigma-Aldrich) was incubated in flow chambers constructed as described previously (Ayloo et al., 2014) for 5 min, followed by blocking with 5% pluronic F-127 (Sigma-Aldrich) for 5 min. Rhodamine-labeled taxol-stabilized microtubules were flowed into the chamber and bound to the anti-tubulin antibody for 10 min. Cell lysates were flowed into the chamber with 10 U/ml hexokinase and 10 mg/ml glucose to scavenge ATP, along with 1 mg/ml BSA, 1 mg/ml casein, 20 μM taxol, 1 mM DTT, and an oxygen-scavenging system (Schroeder et al., 2010). After an initial round of imaging of five locations per chamber, 11 μl wash containing 10 mM MgATP was flowed into the chamber, and each location was re-imaged.

Images were acquired at room temperature using a Nikon TIRF system (PerkinElmer) on an inverted Ti microscope with a 100× objective and an ImagEM C9100-13 camera (Hamamatsu) with Volocity software. Microtubules were randomly chosen from the TIRF field for analysis. GFP fluorescence along the microtubules was measured by line scan using FIJI and corrected for background fluorescence along a line of approximately equal length in the vicinity of the microtubule. Intensity values at least 10% above background were scored to measure the length of the microtubule occupied. Maximum-intensity projections were normalized to the length of the microtubule.

Microtubule co-sedimentation assays were performed on transfected DHC-GFP HeLa cells that were harvested in 80 mM PIPES, 1 mM EGTA, 1 mM $MgCl_2$, and 0.5% Triton X-100 with protease inhibitors. Lysates were centrifuged at 1,000 × *g* and then at 100,000 × *g*. The clarified lysates were combined with 5 mM taxol-stabilized microtubules and/or 10 mM MgATP and incubated at 37°C prior to centrifugation at 39,000 × *g* to pellet the microtubules and bound proteins. Supernatant and pellet fractions were resuspended in denaturing buffer and boiled prior to analysis by SDS-PAGE and western blot.

SUPPLEMENTAL INFORMATION

Supplemental Information includes Supplemental Experimental Procedures, five figures, and one table and can be found with this article online at http://dx.doi.org/10.1016/j.celrep.2015.06.032.

AUTHOR CONTRIBUTIONS

E.K. and E.L.F.H. designed the experiments. E.K. performed all experiments. E.K. and E.L.F.H. analyzed the data and wrote the paper.

ACKNOWLEDGMENTS

This work was supported by NIH pre-doctoral training grant 5T32AG000255 to E.K. and NIH R37 NS060698 to E.L.F.H. We thank Mariko Tokito, Karen Wallace, Swathi Ayloo, and Yvette Wong for their invaluable assistance.

Received: October 23, 2014
Revised: May 6, 2015
Accepted: June 9, 2015
Published: July 9, 2015

REFERENCES

Ayloo, S., Lazarus, J.E., Dodda, A., Tokito, M., Ostap, E.M., and Holzbaur, E.L.F. (2014). Dynactin functions as both a dynamic tether and brake during dynein-driven motility. Nat. Commun. *5*, 4807.

Bilsland, L.G., Sahai, E., Kelly, G., Golding, M., Greensmith, L., and Schiavo, G. (2010). Deficits in axonal transport precede ALS symptoms in vivo. Proc. Natl. Acad. Sci. USA *107*, 20523–20528.

Bradshaw, N.J., Hennah, W., and Soares, D.C. (2013). NDE1 and NDEL1: twin neurodevelopmental proteins with similar 'nature' but different 'nurture'. Biomol Concepts *4*, 447–464.

Cozzolino, M., Pesaresi, M.G., Gerbino, V., Grosskreutz, J., and Carrì, M.T. (2012). Amyotrophic lateral sclerosis: new insights into underlying molecular mechanisms and opportunities for therapeutic intervention. Antioxid. Redox Signal. *17*, 1277–1330.

Dhariwala, F.A., and Rajadhyaksha, M.S. (2008). An unusual member of the Cdk family: Cdk5. Cell. Mol. Neurobiol. *28*, 351–369.

Dhavan, R., and Tsai, L.H. (2001). A decade of CDK5. Nat. Rev. Mol. Cell Biol. *2*, 749–759.

Fu, M.M., and Holzbaur, E.L.F. (2014). Integrated regulation of motor-driven organelle transport by scaffolding proteins. Trends Cell Biol. *24*, 564–574.

Goodwin, P.R., Sasaki, J.M., and Juo, P. (2012). Cyclin-dependent kinase 5 regulates the polarized trafficking of neuropeptide-containing dense-core vesicles in Caenorhabditis elegans motor neurons. J. Neurosci. *32*, 8158–8172.

Hallows, J.L., Chen, K., DePinho, R.A., and Vincent, I. (2003). Decreased cyclin-dependent kinase 5 (cdk5) activity is accompanied by redistribution of cdk5 and cytoskeletal proteins and increased cytoskeletal protein phosphorylation in p35 null mice. J. Neurosci. *23*, 10633–10644.

Hancock, W.O. (2014). Bidirectional cargo transport: moving beyond tug of war. Nat. Rev. Mol. Cell Biol. *15*, 615–628.

Hebbar, S., Mesngon, M.T., Guillotte, A.M., Desai, B., Ayala, R., and Smith, D.S. (2008). Lis1 and Ndel1 influence the timing of nuclear envelope breakdown in neural stem cells. J. Cell Biol. *182*, 1063–1071.

Henriques, A., Pitzer, C., and Schneider, A. (2010). Neurotrophic growth factors for the treatment of amyotrophic lateral sclerosis: where do we stand? Front Neurosci *4*, 32.

Huang, J., Roberts, A.J., Leschziner, A.E., and Reck-Peterson, S.L. (2012). Lis1 acts as a "clutch" between the ATPase and microtubule-binding domains of the dynein motor. Cell *150*, 975–986.

Kiyomitsu, T., and Cheeseman, I.M. (2012). Chromosome- and spindle-pole-derived signals generate an intrinsic code for spindle position and orientation. Nat. Cell Biol. *14*, 311–317.

Klionsky, D.J., Abdalla, F.C., Abeliovich, H., Abraham, R.T., Acevedo-Arozena, A., Adeli, K., Agholme, L., Agnello, M., Agostinis, P., Aguirre-Ghiso, J.A., et al. (2012). Guidelines for the use and interpretation of assays for monitoring autophagy. Autophagy *8*, 445–544.

Kusakawa, G., Saito, T., Onuki, R., Ishiguro, K., Kishimoto, T., and Hisanaga, S. (2000). Calpain-dependent proteolytic cleavage of the p35 cyclin-dependent kinase 5 activator to p25. J. Biol. Chem. *275*, 17166–17172.

Maday, S., Wallace, K.E., and Holzbaur, E.L.F. (2012). Autophagosomes initiate distally and mature during transport toward the cell soma in primary neurons. J. Cell Biol. *196*, 407–417.

Maday, S., Twelvetrees, A.E., Moughamian, A.J., and Holzbaur, E.L.F. (2014). Axonal transport: cargo-specific mechanisms of motility and regulation. Neuron *84*, 292–309.

Magrané, J., Cortez, C., Gan, W.B., and Manfredi, G. (2014). Abnormal mitochondrial transport and morphology are common pathological denominators in SOD1 and TDP43 ALS mouse models. Hum. Mol. Genet. *23*, 1413–1424.

McKenney, R.J., Vershinin, M., Kunwar, A., Vallee, R.B., and Gross, S.P. (2010). LIS1 and NudE induce a persistent dynein force-producing state. Cell *141*, 304–314.

Meijer, L., Borgne, A., Mulner, O., Chong, J.P., Blow, J.J., Inagaki, N., Inagaki, M., Delcros, J.G., and Moulinoux, J.P. (1997). Biochemical and cellular effects of roscovitine, a potent and selective inhibitor of the cyclin-dependent kinases cdc2, cdk2 and cdk5. Eur. J. Biochem. *243*, 527–536.

Menn, B., Bach, S., Blevins, T.L., Campbell, M., Meijer, L., and Timsit, S. (2010). Delayed treatment with systemic (S)-roscovitine provides neuroprotection and inhibits in vivo CDK5 activity increase in animal stroke models. PLoS ONE *5*, e12117.

Mesngon, M.T., Tarricone, C., Hebbar, S., Guillotte, A.M., Schmitt, E.W., Lanier, L., Musacchio, A., King, S.J., and Smith, D.S. (2006). Regulation of cytoplasmic dynein ATPase by Lis1. J. Neurosci. *26*, 2132–2139.

Meuer, K., Suppanz, I.E., Lingor, P., Planchamp, V., Göricke, B., Fichtner, L., Braus, G.H., Dietz, G.P.H., Jakobs, S., Bähr, M., and Weishaupt, J.H. (2007). Cyclin-dependent kinase 5 is an upstream regulator of mitochondrial fission during neuronal apoptosis. Cell Death Differ. *14*, 651–661.

Modi, P.K., Komaravelli, N., Singh, N., and Sharma, P. (2012). Interplay between MEK-ERK signaling, cyclin D1, and cyclin-dependent kinase 5 regulates cell cycle reentry and apoptosis of neurons. Mol. Biol. Cell *23*, 3722–3730.

Morel, M., Authelet, M., Dedecker, R., and Brion, J.P. (2010). Glycogen synthase kinase-3beta and the p25 activator of cyclin dependent kinase 5 increase pausing of mitochondria in neurons. Neuroscience *167*, 1044–1056.

Morfini, G., Szebenyi, G., Brown, H., Pant, H.C., Pigino, G., DeBoer, S., Beffert, U., and Brady, S.T. (2004). A novel CDK5-dependent pathway for regulating GSK3 activity and kinesin-driven motility in neurons. EMBO J. *23*, 2235–2245.

Moughamian, A.J., and Holzbaur, E.L.F. (2012). Dynactin is required for transport initiation from the distal axon. Neuron *74*, 331–343.

Moughamian, A.J., Osborn, G.E., Lazarus, J.E., Maday, S., and Holzbaur, E.L.F. (2013). Ordered recruitment of dynactin to the microtubule plus-end is required for efficient initiation of retrograde axonal transport. J. Neurosci. *33*, 13190–13203.

Nguyen, M.D., Larivière, R.C., and Julien, J.P. (2001). Deregulation of Cdk5 in a mouse model of ALS: toxicity alleviated by perikaryal neurofilament inclusions. Neuron *30*, 135–147.

Niethammer, M., Smith, D.S., Ayala, R., Peng, J., Ko, J., Lee, M.S., Morabito, M., and Tsai, L.H. (2000). NUDEL is a novel Cdk5 substrate that associates with LIS1 and cytoplasmic dynein. Neuron *28*, 697–711.

Nikolic, M., Dudek, H., Kwon, Y.T., Ramos, Y.F., and Tsai, L.H. (1996). The cdk5/p35 kinase is essential for neurite outgrowth during neuronal differentiation. Genes Dev. *10*, 816–825.

Ou, C.-Y., Poon, V.Y., Maeder, C.I., Watanabe, S., Lehrman, E.K., Fu, A.K.Y., Park, M., Fu, W.-Y., Jorgensen, E.M., Ip, N.Y., and Shen, K. (2010). Two cyclin-dependent kinase pathways are essential for polarized trafficking of presynaptic components. Cell *141*, 846–858.

Pandey, J.P., and Smith, D.S. (2011). A Cdk5-dependent switch regulates Lis1/Ndel1/dynein-driven organelle transport in adult axons. J. Neurosci. *31*, 17207–17219.

Patrick, G.N., Zhou, P., Kwon, Y.T., Howley, P.M., and Tsai, L.-H. (1998). p35, the neuronal-specific activator of cyclin-dependent kinase 5 (Cdk5) is degraded by the ubiquitin-proteasome pathway. J. Biol. Chem. *273*, 24057–24064.

Perlson, E., Jeong, G.-B., Ross, J.L., Dixit, R., Wallace, K.E., Kalb, R.G., and Holzbaur, E.L.F. (2009). A switch in retrograde signaling from survival to stress in rapid-onset neurodegeneration. J. Neurosci. *29*, 9903–9917.

Schroeder, H.W., 3rd, Mitchell, C., Shuman, H., Holzbaur, E.L.F., and Goldman, Y.E. (2010). Motor number controls cargo switching at actin-microtubule intersections in vitro. Curr. Biol. *20*, 687–696.

Shukla, V., Skuntz, S., and Pant, H.C. (2012). Deregulated Cdk5 activity is involved in inducing Alzheimer's disease. Arch. Med. Res. *43*, 655–662.

Su, S.C., and Tsai, L.-H. (2011). Cyclin-dependent kinases in brain development and disease. Annu. Rev. Cell Dev. Biol. *27*, 465–491.

Tsai, L.H., Takahashi, T., Caviness, V.S., Jr., and Harlow, E. (1993). Activity and expression pattern of cyclin-dependent kinase 5 in the embryonic mouse nervous system. Development *119*, 1029–1040.

Wynshaw-Boris, A. (2007). Lissencephaly and LIS1: insights into the molecular mechanisms of neuronal migration and development. Clin. Genet. *72*, 296–304.

Zhang, L., Liu, W., Szumlinski, K.K., and Lew, J. (2012). p10, the N-terminal domain of p35, protects against CDK5/p25-induced neurotoxicity. Proc. Natl. Acad. Sci. USA *109*, 20041–20046.

Zheng, Y.-L., Li, B.-S., Kanungo, J., Kesavapany, S., Amin, N., Grant, P., and Pant, H.C. (2007). Cdk5 Modulation of mitogen-activated protein kinase signaling regulates neuronal survival. Mol. Biol. Cell *18*, 404–413.

Zyłkiewicz, E., Kijańska, M., Choi, W.-C., Derewenda, U., Derewenda, Z.S., and Stukenberg, P.T. (2011). The N-terminal coiled-coil of Ndel1 is a regulated scaffold that recruits LIS1 to dynein. J. Cell Biol. *192*, 433–445.